BNL-28041
AMD-857

ON TWO APPROACHES TO 3D RECONSTRUCTION IN NMR ZEUGMATOGRAPHY*

CONF-800247--1

Robert B. Marr

Applied Mathematics Department
Brookhaven National Laboratory
Upton, New York 11973

Ching-Nien Chen

Department of Chemistry
State University of New York at Stony Brook
Stony Brook, New York 11974

Paul C. Lauterbur

Departments of Chemistry and Radiology
State University of New York at Stony Brook
Stony Brook, New York 11974

To Appear In

"Lecture Notes in Medical Informatics"
Springer-Verlag, publisher

As Part Of

Proceedings of a Conference on
Mathematical Aspects of Computerized Tomography

Held At

Mathematisches Forschungsinstitut
Oberwolfach, West Germany
February 10-16, 1980

*Work at Brookhaven supported by contract DE-AC02-76CH00016 with the U. S. Department of Energy.

Work at Stony Brook partially supported by Grant No. CA-153000 awarded by the National Cancer Institute, DHEW and by Grant No. HL19851OA1, awarded by the National Heart, Lung and Blood Institute, DHEW. Based in part on a dissertation submitted by C.-N. Chen in partial fulfillment of the requirements for the ph.D. degree (Stony Brook, 1980).

ON TWO APPROACHES TO 3D RECONSTRUCTION IN NMR ZEUGMATOGRAPHY*

Robert B. Marr

Applied Mathematics Department
Brookhaven National Laboratory
Upton, New York 11973

Ching-Nien Chen

Department of Chemistry
State University of New York at Stony Brook
Stony Brook, New York 11974

Paul C. Lauterbur

Departments of Chemistry and Radiology
State University of New York at Stony Brook
Stony Brook, New York 11974

ABSTRACT

In nuclear magnetic resonance (NMR) zeugmatography, the primary data pertain to integrals of the unknown nuclear spin density $f(x,y,z)$ over planes instead of lines in R^3. Two "natural" approaches to reconstructing f from such data are: (1) By numerical implementation of the inverse Radon transform in three dimensions (the direct approach), and (2) by application, in two successive stages, of existing well-known algorithms for inverting the two-dimensional Radon transform (the two-stage approach). These two approaches are discussed and compared, both from a theoretical standpoint and through computer results obtained with real NMR data. For the cases studied to date the two methods appear to produce qualitatively similar results.

Introduction - A Brief Primer on NMR

Nuclear magnetic resonance (NMR) is a phenomenon arising from the fact that certain atomic nuclei possess both an intrinsic angular momentum (or "spin"), which we denote here as $\underline{S}$, and an intrinsic magnetic moment, $\underline{\mu} = \gamma \cdot \underline{S}$, where the "magnetogyric ratio", γ, is a constant characteristic of the nuclear species. In the presence of a magnetic field, $\underline{B}(t)$, the classical (pre-quantum) behavior of such a system is

*Work at Brookhaven supported by contract DE-AC02-76CH00016 with the U.S. Department of Energy.

Work at Stony Brook partially supported by Grant No. CA-153000 awarded by the National Cancer Institute, DHEW, and by Grant No. HL19851O1A1, awarded by the National Heart, Lung and Blood Institute, DHEW. Based in part on a dissertation submitted by C-N. Chen in partial fulfillment of the requirements for the Ph.D. degree (Stony Brook, 1980).

governed by the vector equation of motion, $\dot{\underline{S}}$ = torque = $\underline{\mu} \times \underline{B}$; in particular, if $\underline{B}(t) = \underline{B}_0 = \text{const.}$, gyroscopic precession of $\underline{S}$ about the direction of $\underline{B}_0$ is predicted, with a frequency ν_0 given by the Larmor formula, $\nu_0 = \gamma \cdot |\underline{B}_0|/2\pi$. In the more appropriate quantum mechanical description, the same quantity ν_0 emerges as the frequency at which quanta of the electromagnetic field (photons) are emitted or absorbed when the nucleus undergoes transitions between adjacent levels in the discrete energy spectrum associated with the coupling, $E = \underline{\mu} \cdot \underline{B}_0$ between its spin and the static field $\underline{B}_0$. Now the key point is that with a static field strength of the order of 0.1 to 10 tesla (1 to 100 kilogauss), which is easily achieved in the laboratory and sufficiently high to prevail over local magnetic fields within most materials, the Larmor frequency ν_0 is in the radio frequency (rf) range, corresponding to photon wavelengths which are several orders of magnitude larger than any object one is likely to be studying in the laboratory. Consequently, the macroscopic ensemble consisting of all the spins associated with a particular nuclear species within the object interacts coherently with an applied rf magnetic field $\underline{B}_1(t)$ (directed perpendicular to $\underline{B}_0$), producing resonance phenomena at frequencies of the applied field near ν_0. It also turns out that, in most materials of interest at room temperature, the relaxation times, which characterize the rates at which the spin ensemble approaches equilibrium within itself and with its environment, are sufficiently large compared with the period of precession, $1/\nu_0$, to permit these resonance phenomena to be detected and studied.

In conventional NMR, a research tool of venerable (> 25 years) standing which provides much useful information concerning the structure of matter, the applied static field $\underline{B}_0$ is by design kept highly homogeneous in its spatial dependence, so that the "fine structure" of the resonance can be used to make inferences concerning the variations in magnetic field occurring at the submicroscopic scale within the material. (Ref. [1] is the most recent text on this subject.) In NMR zeugmatography (the word was coined from a Greek word meaning "that which joins together"--see [2]), $\underline{B}_0$ varies with position, permitting information concerning the density $f(x,y,z) = f(\underline{r})$ of a given nuclide as a function of position to be obtained (as a result of the nuclei's coupling--or "joining together"--the two fields $\underline{B}_0$ and $\underline{B}_1(t)$). In a typical zeugmatography measurement, the data pertain (directly, or indirectly in ways we discuss below) to integrals of $f(\underline{r})$ over surfaces of constant $\underline{B}_0$; the apparatus can be designed so that these surfaces are very nearly parallel planes with an orientation that is under the control of the experimenter. Thus, the Radon transform of the three dimensional density function can in principle be sampled as closely as one likes. (The Appendix to ref. [3] contains a Bibliography on NMR Zeugmatographic Imaging and Related Techniques--reasonably comprehensive through 1978. For more recent work, the literature cited in ref. [4] may be helpful.)

The most recently completed NMR zeugmatographic device at Stony Brook is shown in Figure 1, which may serve to illustrate some of the foregoing concepts in more

practical terms. The large magnet is designed to produce a homogeneous field $\underline{B}_{00}$ of 0.1 tesla (1 kilogauss) within a region near the center of the cylindrical bore. The spatial variation of $\underline{B}_0(\underline{r})$ is achieved by superimposing on $\underline{B}_{00}$ an inhomogeneous field, $\Delta\underline{B}_0(\underline{r})$ (much smaller in magnitude than $\underline{B}_{00}$), produced by the "gradient coils" in the open structure surrounding the large magnet; these are specially designed so that the relevant component of $\Delta\underline{B}_0(r)$--namely, the component along the direction of $\underline{B}_{00}$--can attain a gradient in any desired direction which is essentially constant throughout the initially homogeneous region. At the center of the photograph, within the bore of the magnet, can be seen in end view the cylindrical form upon which is wound the coil used for transmission of the rf magnetic field $\underline{B}_1$, as well as for detection of the resultant signal. The interior of this coil constitutes the "sensitive volume" for this apparatus.

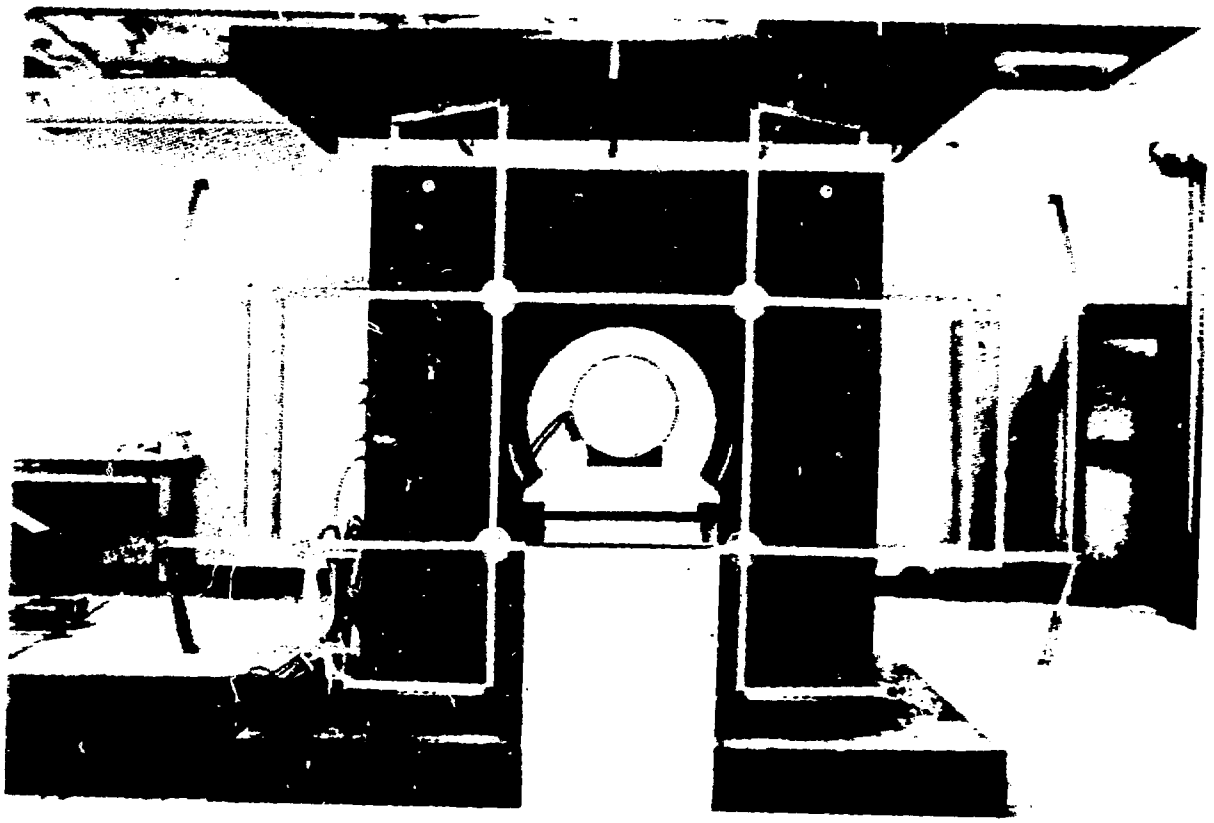

Figure 1. A body-size magnet at Stony Brook. The direction of the homogeneous field is parallel to the axis of the cylindrical bore, which is 52 cm in diameter. Linear field gradients are produced by circuits mounted in the open structure. The probe which transmits rf pulses and receives nuclear FID signals is built on a cylindrical form located in the middle of the bore.

With both conventional and zeugmatographic NMR devices, one wishes to measure a certain function--let us call it $A(\nu)$--which measures the strength of the resonance response as a function of applied frequency, ν. In each case, there are various experimental procedures available for carrying this out: In CW NMR, a weak, sinusoidally varying rf signal is applied, and the frequency ν of this signal is varied slowly as the resonance response is recorded. This seemingly straightforward method has the major disadvantage that at each instant of time only a small fraction of the nuclei within the ensemble are contributing useful information; consequently, the total time required to obtain data at a reasonable signal-to-noise ratio for the kind of frequency range which is typically of interest is inordinately large. For this reason, it is more common in practice to utilize any of a number of possible pulsed NMR techniques [5]. The simplest of these conceptually, and the one used to obtain the data on which the results to be presented below are based, consists of applying a single strong rf pulse, of sufficiently short duration that its Fourier transform is nearly constant throughout the frequency band of interest. The so-called free induction decay (FID) of a spin ensemble excited in this fashion induces in the receiver coil an rf signal which (as a function of time after the pulse) can be described as the inverse Fourier transform of $A(\nu)$, multiplied by an exponentially decreasing function. (The latter is associated with the loss of phase coherence as the spin-spin interactions bring the ensemble to statistical equilibrium.) In effect, therefore, the function $A(\nu)$ is determined by the FID to some degree of resolution--limited, among other things, by the finite relaxation time for the exponential decay. In the zeugmatographic situation previously described, with a constant static field gradient of known direction and magnitude, the function $A(\nu)$ so obtained is, after introduction of the appropriate linear relationship between ν and distance along the field gradient, a representation of the one-dimensional projection of $f(\underline{r})$ onto that direction. It will be noted that the spatial resolution associated with this measurement is determined by the aforementioned frequency resolution of $A(\nu)$, as well as by the magnitude of the field gradient.

As already indicated, there exist a number of other pulsed NMR techniques, and these, in combination with various schemes for altering the field gradient during the measurement, yield a large variety of possible ways for collecting zeugmatographic data. In principle, line integrals of f, or even the values of f at individual points can be directly measured, albeit at low efficiency. In the following, however, we shall assume that the data is obtained in one of the ways already described and presented in the form of some finite set of 1D projections of f.

The problem of determining $f(x,y,z)$ from its plane integrals was among those posed and solved analytically by Radon [6], and the possibility of applying this result in an image reconstruction context was discussed several years ago by Cormack [7]. In previously reported work on 3D reconstruction from NMR data [8,9], the method actually used was not of this 'direct' type suggested by Radon's formula, but instead

used a 2D reconstruction algorithm--first to obtain from the data a set of 2D projections of the object, and then, in a separate stage of processing, to obtain a set of parallel cross-sections of the object, as in standard CT. More recently, the direct method has been implemented by Chen [10,11] and independently by Shepp [12]. In the following, we shall examine the "two stage" method as well as the direct method more closely.

Rationale for the Direct and Two Stage Methods of Reconstruction

The Radon transform, $\hat{f} = Rf$, of a function f on $\mathbb{R}^3$ is defined so that for any real s and unit vector $\underline{\omega} = \langle \omega_1, \omega_2, \omega_3 \rangle$, $(\omega_1^2+\omega_2^2+\omega_3^2 = 1)$, $\hat{f}(s,\underline{\omega})$ is the integral of $f(\underline{r}) = f(x,y,z)$ over the plane, $\{\underline{r} \in \mathbb{R}^3 : \underline{r}\cdot\underline{\omega} = s\}$. This same integral will also be denoted as $(P_{\underline{\omega}} f)(s)$ and the function $(P_{\underline{\omega}} f)$ will be referred to as the 1D projection of f associated with the direction $\underline{\omega}$. Thus

$$\hat{f}(s,\underline{\omega}) = (P_{\underline{\omega}} f)(s) = \int f(\underline{r})\delta(s-\underline{r}\cdot\underline{\omega})d^3\underline{r} \tag{1}$$

where δ is the Dirac delta function.

Introducing standard spherical coordinates, θ = "co-latitude", and φ = azimuth, to label the directions $\underline{\omega}$, so that

$$\underline{\omega}_{\theta,\varphi} = \langle \cos\varphi \sin\theta,\ \sin\varphi \sin\theta,\ \cos\theta \rangle, \tag{2}$$

we obtain, after change of integration variables, the formula,

$$\begin{aligned} \hat{f}(s,\omega_{\theta,\varphi}) &\equiv (P_{[\theta,\varphi]} f)(s) \\ &= \int g_{\varphi}(s \sin\theta - v \cos\theta, s \cos\theta + v \sin\theta)dv \end{aligned} \tag{3}$$

where

$$g_{\varphi}(t,z) = \int f(t \cos\varphi - u \sin\varphi,\ t \sin\varphi + u \cos\varphi,\ z)du \tag{4}$$

Equations (3) and (4) each have the form of a two-dimensional Radon transformation with respect to some pair of variables. Explicitly, if we define the function $P_\alpha g$ by:

$$\begin{aligned} (P_\alpha g)(s,\ldots) &= \int g(s \cos\alpha - t \sin\alpha,\ s \sin\alpha + t \cos\alpha, \ldots)dt \\ &= \iint g(x,y,\ldots)\ \delta(s - x \cos\alpha - y \sin\alpha)dxdy, \end{aligned} \tag{5}$$

for any angle α, and any function $g(x,y,\ldots)$ of two or more variables, then (3) and (4) can be summarized in the succinct form,

$$(P_{[\theta,\varphi]} f)(s) = (P_s(P_\varphi f))(s) \tag{6}$$

where $\bar{\theta} = \pi/2 - \theta$. Eq. (6) expresses formally what is obvious geometrically--namely, that the planar integrals of eq. (1) can be obtained by first integrating along lines parallel to the X-Y plane in order to form the two-dimensional projections (or "X-rays") of f for all such directions, and then line integrating the 2D projections so obtained. Note that the function $g_\varphi = P_\varphi f$, of eq. (4) is the 2D projection of f for parallel rays in the direction, $(\sin\varphi, -\cos\varphi, 0)$.

Essentially, the two-stage method of reconstruction is based on eq. (6) and some scheme for numerically approximating the inverse of the transformation, $g \to P_\alpha g$, of eq. (5). This inverse can be expressed analytically by the well-known formula,

$$g(x,y,\ldots) = \frac{1}{2\pi^2}\int_0^\pi d\alpha\, P\int_{-\infty}^{\infty} \frac{\frac{d}{ds}(P_\alpha g)(s)ds}{x\cos\alpha + y\sin\alpha - s} \qquad (7)$$

where P denotes Cauchy principal value.

On the other hand, the 3D Radon transformation, eq. (1), has the inversion formula [13],

$$f(\underline{r}) = \frac{-1}{8\pi^2}\int_{\underline{\omega}\,\in\,\text{unit sphere}} d^2\underline{\omega}\cdot\left[\frac{d^2}{ds^2}(P_{\underline{\omega}}f)(s)\right]\Big|_{s=\underline{r}\cdot\underline{\omega}}, \qquad (8)$$

and this provides the theoretical basis for the direct method of reconstruction. Obviously, the two analytically exact schemes must be equivalent (this will be demonstrated presently), but this assertion may not hold for practical implementations of the two methods.

It should be noted that, in contrast with eq. (7), the direct inversion formula for the 3D case, eq. (8), is local--that is, to recover f at a point $\underline{r}$, one needs the values of $(Rf)(s,\underline{\omega})$ only for planes $(s,\underline{\omega})$ passing infinitesimally close to $\underline{r}$.

Direct and Two Stage Convolution Algorithms

We assume that the given data consists of a sampling of $(P_{\underline{\omega}}f)(s)$ on a uniform linear mesh of points, $s = \ell \cdot a$, $\ell = 0, \pm1, \pm2, \ldots$, for some finite set of directions, $\underline{\omega}$. Such data is well suited to the use of convolution (or "filtered back-projection") algorithms, and we accordingly confine our attention to the direct and two-stage versions of this type of algorithm. We assume that the unknown density f is "essentially" band limited at a spatial frequency W not exceeding the Nyquist frequency, π/a.

The direct approach could in principle be adapted to arbitrary sets of directions, but to accommodate the two-stage approach, the available directions must comprise a "spherical-rectangular" mesh of the form:

$$\underline{\omega} = \underline{\omega}_{j,k} = (\theta_j, \varphi_k); \tag{9}$$

for simplicity, we furthermore consider only the case of uniformly spaced angular coordinates:

$$\theta_j = (j+\tfrac{1}{2})\pi/J \ , \ 0 \le j < J \ ; \ \varphi_k = (k+\tfrac{1}{2})\pi/K, \ 0 \le k < K. \tag{10}$$

With this choice of directions, the two-stage method is considerably simplified (uniform angular spacing is involved at each stage of 2D reconstruction), but the choice is evidently not 'optimal' as the density of points on the sphere varies like $1/\sin\theta$. We denote the data elements by $G(j,k,\ell)$, which we take to be in dimensionless form so that

$$G(j,k,\ell) \doteq a\left[(P_{[\theta_j,\varphi_k]}f)(\ell\cdot a)\right] \tag{11}$$

The function, f_D, resulting from a convolution algorithm of the <u>direct</u> type can now be written:

$$f_D(x,y,z) = \frac{1}{4JK}\sum_{j,k,\ell} \sin\theta_j \ \psi(\underline{r}\cdot\underline{\omega}_{jk}-a\cdot\ell)\ G(j,k,\ell) \tag{12}$$

where

$$\underline{r}\cdot\underline{\omega}_{jk} = (x\cos\varphi_k + y\sin\varphi_k)\sin\theta_j + z\cos\theta_j, \tag{13}$$

and where the convolvent ψ is an even, real-valued function--

$$\psi(s) = \psi(-s) = \text{real} \ , \ \text{all } s \text{ --} \tag{14}$$

such that the corresponding "filter function,"

$$\Psi = F\,\psi = \text{Fourier transform of } \psi, \tag{15}$$

satisfies

$$\Psi(\xi) = \xi^2 \quad \text{for } |\xi| < W. \tag{16}$$

In eq. (12), the factor

$$\frac{\sin\theta_j}{4JK} = \frac{1}{4\pi^2}\sin\theta_j(\Delta\theta)_j\cdot(\Delta\varphi)_k \doteq \frac{(\Delta\omega)_{j,k}}{4\pi^2} \tag{17}$$

is needed in order that a filter function Ψ independent of (j,k) and satisfying eq. (16) can justifiably be used. We do not consider here the more general possibility, discussed by Davison and Grunbaum [14,15] of introducing distinct filter func-

tions for each direction, determined according to a general optimality criterion In the two-stage method, the 2D projections, $g_{\varphi_k}(t,z)$, $0 \le k < K$, which are reconstructed in Stage I, can in practical terms be computed at only a finite number of points (t,z). The z-values used can be chosen freely according to which planes, z = constant, are selected for the final reconstruction, but the t-values must be equally spaced to expedite use of the convolution algorithm in Stage II. Although the sampling interval, a, of the original data could normally be used here as well, we wish to allow for the possibility of a smaller spacing, and shall accordingly assume that the t-values used are: $t = m \cdot b$, $m = 0, \pm 1, \pm 2, \ldots$, with $b \le a$. Then the function, f_{2S}, computed with a two-stage convolution algorithm can be written:

$$f_{2S}(x,y,z) = \frac{b}{2K} \sum_{k,m} \phi_2(x\cos\varphi_k + y\sin\varphi_k - mb)\, g_{\varphi_k}(mb,z), \tag{18}$$

where (for arbitrary t and z)

$$g_{\varphi_k}(t,z) = \frac{1}{2J} \sum_{j,\ell} \phi_1(t\sin\theta_j + z\cos\theta_j - \ell a)\cdot G(j,k,\ell), \tag{19}$$

and where the convolvents ϕ_1 and ϕ_2 (normally they would be the same) are even, real-valued functions with Fourier transforms Φ_1 and Φ_2 satisfying

$$\Phi_{\binom{1}{2}}(\xi) = |\xi| \text{ for } |\xi| < W. \tag{20}$$

Theoretical comparison

First we consider the two-stage algorithm in the limit, $b \to 0$, where eq. (18) becomes:

$$f_{2S}(x,y,z)\Big|_{b=0} = \frac{1}{2K} \sum_k \int \phi_2(x\cos\varphi_k + y\sin\varphi_k - t)\cdot g_{\varphi_k}(t,z)dt. \tag{21}$$

This leads, after substitution of eq. (19) and carrying out a change of integration variable, to the result

$$f_{2S}(x,y,z)\Big|_{b=0} = \frac{1}{4JK} \sum_{j,k,\ell} \sin\theta_j\, \psi^{(2S)}_{\theta_j}(\underline{r}\cdot\underline{\omega}_{jk} - \ell\cdot a)G(j,k,\ell). \tag{22}$$

where

$$\psi^{(2S)}_{\vartheta}(s) = \frac{1}{\sin\theta} \int dt\, \phi_1(s - t\sin\theta)\phi_2(t), \tag{23}$$

with Fourier transform,

$$\psi_\theta^{(2S)}(\xi) = \phi_1(\xi) \cdot \left(\frac{\phi_2(\xi \sin\theta)}{\sin\theta}\right). \qquad (24)$$

Thus, in the limit of infinitely refined sampling of the intermediate 2D projections, the two-stage algorithm is equivalent to the direct algorithm, eq. (12), using for ψ the function $\psi_\theta^{(2S)}$ defined by eq. (24). We note that, if ϕ_1 and ϕ_2 satisfy eq. (20) then $\psi_\theta^{(2S)}$ satisfies eq. (16) as required; for $W \to \infty$, this demonstrates the exact equivalence of the two analytic forms for expressing the inverse Radon transform, as discussed earlier. It is evident that any dependence of $\psi_\theta^{(2S)}$ on θ is confined to higher spatial frequencies, and is related to the manner in which ϕ_1 and ϕ_2 are 'rolled off'; in particular, if sharply cut-off (Ram-Lak) filters, $\phi_{1,2}$, are used, then $\psi_\theta^{(2S)}$ is a truncated parabola, strictly independent of θ.

In the more realistic situation with $0 < b \leq a$, we obtain instead of eqs. (22) and (23), the result,

$$f_{2S}(x,y,z) = \frac{1}{4JK} \sum_{j,k,\ell} G(j,k,\ell) \times$$

$$\times \left\{ b \sum_{n=-\infty}^{\infty} \phi_2(n\cdot b+\delta)\, \phi_1(s-(n\cdot b+\delta)\sin\theta_j) \right\}\Big|_{s=\underline{r}\cdot\underline{\omega}_{jk}-\ell\cdot a} \qquad (25)$$

where δ [$= \delta(x,y,b,\varphi_k)$] is the distance between $(x\cos\varphi_k + y\sin\varphi_k)$ and the nearest mesh point, $t = m \cdot b$ --that is,

$$\left(\frac{x\cos\varphi_k + y\sin\varphi_k}{b}\right) = \text{integer} + \frac{\delta}{b}, \qquad -\frac{1}{2} \leq \frac{\delta}{b} < \frac{1}{2}. \qquad (26)$$

Now if the functions ϕ_1 and ϕ_2 were both strictly band-limited at the Nyquist frequency, so that

$$\phi_1(\xi) = \phi_2(\xi) = 0 \quad \text{for } |\xi| \geq \frac{\pi}{b}, \qquad (27)$$

then it would follow from $\sin\theta_j \leq 1$ and Poisson's sum formula that the right-hand sides of eqs. (22) and (25) are in fact the same, independent of the values of δ and b. In practical implementations of convolution algorithms, because the methods used for interpolating between mesh points must be kept computationally simple, eq. (27) is never satisfied in a rigorous sense, and some differences between the direct and two-stage methods due to "intermediate discretization error" in the latter method may therefore be expected to exist. We shall not explore this further here except to note that this effect is apparently also confined to the higher spatial frequencies.

On the Choice of Filter Functions

The convolution method is usually implemented with a discretized form of the desired convolution, combined with some interpolation scheme for obtaining the intermediate values needed during back-projection. Consequently, as is well-known, filter functions, $\Phi = F\phi$, encountered in practice generally have the form

$$\Phi(\xi) = I(\xi) \cdot \mathring{\phi}(\xi) \tag{28}$$

where $I(\xi)$ is determined by the interpolation method used, and where $\mathring{\phi}(\xi)$ is a periodic function, given by the cosine series,

$$\mathring{\phi}(\xi) = a \cdot C_0 + 2a \sum_{\ell=1}^{\infty} C_\ell \cos(\ell a \xi), \qquad \left[= \mathring{\phi}(\xi + \tfrac{2\pi}{a})\right], \text{ all } \xi, \tag{29}$$

in which $C_\ell = C_{-\ell} = \phi(\pm \ell a)$, $\ell = 0, 1, 2, \ldots$, are the coefficients which define the discrete convolution, and 'a' denotes spacing between mesh points. Our implementations of both the direct and two-stage methods have for the most part made use of simple linear interpolation, for which

$$I(\xi) = \operatorname{sinc}^2(a\xi/2\pi) = \frac{4 \sin^2(a\xi/2)}{(a\xi)^2}, \tag{30}$$

and this will be assumed throughout in what follows.

In our investigations to date with the <u>two-stage</u> method, we have used either the <u>Ram-Lak</u> filter [16], defined by

$$\mathring{\phi}(\xi) = |\xi|, \quad \text{for } |\xi| \le \frac{\pi}{a}, \tag{31}$$

with coefficients,

$$C_\ell = \begin{cases} \frac{\pi}{2a^2} & \ldots \ell = 0 \\ \frac{-2}{\pi^2 a^2 \ell^2} & \ldots \ell \text{ odd} \\ 0 & \ldots \text{otherwise,} \end{cases} \tag{32}$$

or the <u>Shepp-Logan</u> filter [17], for which

$$\mathring{\phi}(\xi) = \frac{2}{a} \left|\sin(a\xi/2)\right|, \tag{33}$$

and

$$C_\ell = -\frac{4}{\pi a^2(4\ell^2-1)} . \tag{34}$$

For the filter, $\Psi = I \cdot \overset{\bullet}{\Psi}$, of the direct method, several alternatives were at first considered, but the only one which has been extensively tested is the "three-point" filter defined by

$$\overset{\circ}{\Psi}(\xi) = \frac{2}{a^2}[1 - \cos(a\xi)], \tag{35}$$

with three non-vanishing coefficients,

$$C_0 = \frac{2}{a^3} , \; C_{\pm 1} = -\frac{1}{a^3} , \qquad C_\ell = 0 \text{ for } |\ell| > 1. \tag{36}$$

The associated discrete convolution is identical with the standard central second difference approximation, $-\delta^2$, to the operator, $\frac{-d^2}{ds^2}$, appearing in eq. (8), in agreement with the algorithm used by Shepp [12]. It is noteworthy that

$$\overset{\circ}{\Psi}_{3\text{-point}} = \left[\overset{\bullet}{\Psi}_{\text{Shepp-Logan}}\right]^2 , \tag{37}$$

or in other words that, as an operator on the space of sequences, discrete Shepp-Logan convolution is the (positive) square root of $-\delta^2$.

The analogous function $\overset{\circ}{\Psi}$ constructed from the Ram-Lak filter--namely, the truncated parabola,

$$\overset{\circ}{\Psi}(\xi) = \xi^2 \quad \text{for} \quad |\xi| \le \pi/a \text{ --} \tag{38}$$

results in an infinite set of nonvanishing coefficients,

$$C_0 = \frac{\pi^2}{3a^3} , \; C_\ell = \frac{2\cdot(-1)^\ell}{a^3\cdot\ell^2} \quad \text{for} \quad \ell \neq 0. \tag{39}$$

This filter is obviously less attractive to implement and does not preserve the locality property of the inversion formula (8), as does the three-point filter.

Experimental Comparison

For comparison purposes, experimental data originally obtained by Lauterbur and Lai [9] were reprocessed with both two-stage and direct convolution algorithms.

The magnet in these experiments was operated at a field strength of 0.0938 tesla (938 gauss) and the magnitude of the superimposed linear gradient was 4.7×10^{-6} tesla (47 milligauss) per centimeter. The density function under investigation was that of protons (hydrogen nuclei), which resonate at 4.00 MHz in a static field of the stated strength. The spherical coordinates, θ and φ, defining the field gradient direction were each stepped from 6° to 354° in 12° increments under the control of an automatic 3D vector gradient generator [18], resulting in a total of $(\frac{30}{2}) \times (\frac{30}{2}) = 225$ inequivalent directions. (The use of anti-parallel pairs of directions is desirable in order to minimize certain experimental errors which are present. The additional two-fold redundancy in these experiments simply had the effect of improving the final signal-to-noise ratio.) The corresponding one-dimensional projections were obtained by recording in digital form, and then Fourier transforming, the free induction decays (FID's) following 4.00 Mhz rf pulses. For this purpose, 1024 points were used for each FID. After proper centering and averaging each of the 900 1D projections so obtained was reduced to a 33 point array for input to the reconstruction algorithms.

One of the objects studied was a phantom consisting of seven vials of aqueous $NiCl_2$ solution, arranged in distinctive patterns on three separate layers as shown in Fig. 2a. Figure 2b depicts the relative density of protons within the three layers (on the planes numbered 12, 16, and 20 in Fig. 5 of ref. [9]), as reconstructed in ref. [9] using the two-stage method with Ram-Lak filtering. The intermediate 2D projections were thirty in number, each digitized as a 33 × 33 pixel array. Figure 2c was computed in exactly the same way, except that Shepp-Logan filtering was used. The result obtained from the same data by the direct method with three-point filtering is shown in Fig. 2d. The small but visible differences in the reconstructed background levels in Figs. 2b and 2c--especially in the latter--may have arisen from the use of truncated versions of the 2D convolution algorithms as they were actually implemented, but the effect is not as yet fully understood and is being investigated further.

The other object studied in ref. [9], using essentially the same experimental procedures, was a nectarine. A comparison of results from the two-stage /Ram-Lak and direct/three-point reconstruction algorithms applied to the nectarine data is provided in Fig. 3.

In addition to the aforementioned studies, other comparative studies, with simulated as well as real data, have been carried out. These will be reported upon in a more complete account of this work which is being prepared [11].

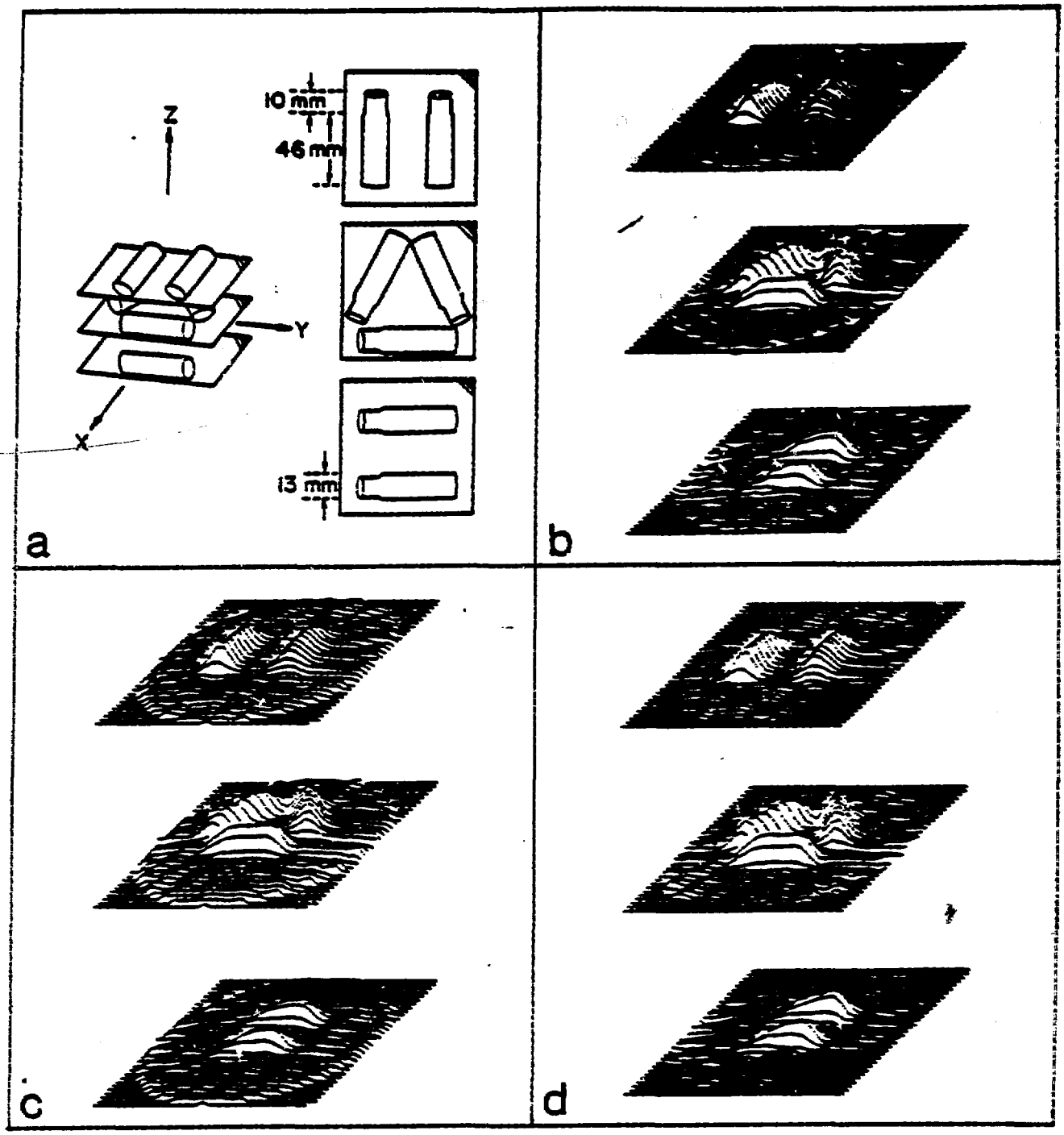

Figure 2. (a) Sketch of the arrangement and dimensions of the phantom used in the seven vial experiment. The homogeneous field of the main magnet pointed in the +Z direction. Reconstructed densities on three of the thirty three tomographic planes used are shown for: (b) two-stage method with Ram-Lak filter, (c) two-stage method with Shepp-Logan filter, and (d) direct method using the three-point filter. Elevations in the plots indicate relative densities. Each plot was prepared from an array of 33 x 33 pixels.

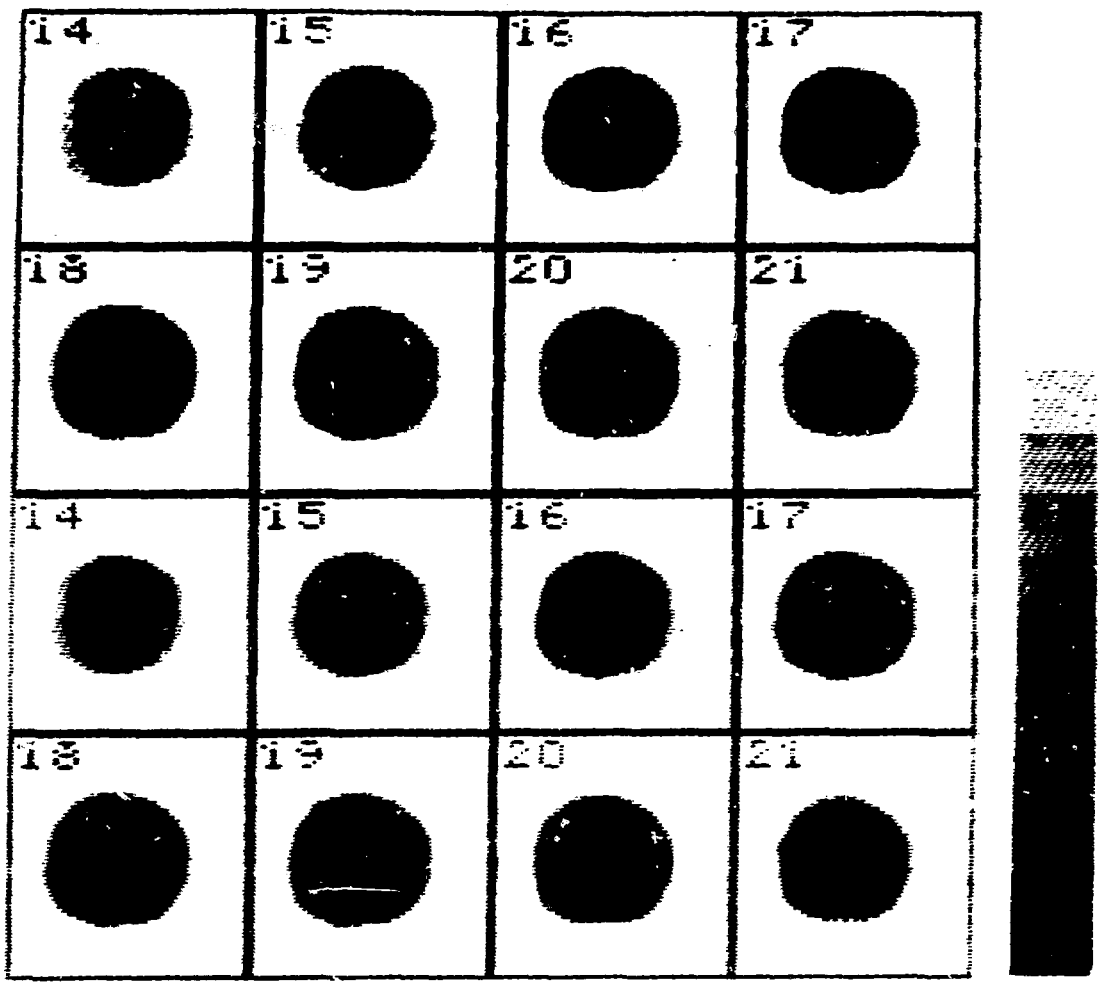

Figure 3. Eight slices from 3D images of a nectarine as reconstructed by the two-stage method with Ram-Lak filtering (top two rows, reproduced from ref. [9]), and by the direct method with three-point filtering (bottom two rows).

Discussion

The direct and two-stage methods have both been established as practical techniques for obtaining NMR zeugmatographic images, and they seem to yield nearly equivalent results for the range of examples studied thus far. In other respects, however, there are significant differences between the two methods which may be mentioned here. Unlike the two-stage method, the direct method places no constraint such as eq. (3) on the choice of directions $\underline{\omega}$ to be used in an experiment, so that once the number of such directions has been fixed, they could in principle be located so as to maximize the final spatial resolution [15]. In addition, the direct method, but evidently not the two-stage method, can be implemented so that the important property of locality possessed by the exact formula (8) remains essentially intact.

This is reflected in the success of the simple three-point filter, eq. (36), and implies that a sufficiently small restricted region of interest within the complete object can be reconstructed with much greater efficiency using the direct method, (Note that only a correspondingly small portion of each 1D projection is needed in such situations.) On the other hand, with $JxK = N^2$ 1D-projections, the back-projections involved in reconstructing an image of N^3 voxels seem to require $\sim N^3 x N^2 = N^5$ steps with the direct method and only $\sim 2N^4$ steps with the two-stage method, so that when the entire object (or any substantial portion of it) must be reconstructed, the two stage method seems to have an overwhelming advantage computationally.

The latter observation has been borne out in our experience with the two methods but deserves closer examination: The reason for the different computational complexities, apparently, is that the two-stage method is structured to take advantage of the special nature of the angular grid, eq. (9), whereas the direct method, in the general form described, is not. The remedy which now suggests itself is to implement the 3D back-projection (that is, the double summation over the indices j and k in eq. (12) for the N^3 different points (x,y,z)) in such a way that it emulates the procedure used by the two stage algorithm -- with an intermediate set of 2D images and two separate interpolation steps, but with no second stage of filtering. The resulting "hybrid" method, retains the locality property of the direct method and should require less computing time than the original two-stage method. This method is currently being implemented and will be reported upon elsewhere. [11]

References

1. M. L. Martin, G. J. Martin, and J. J. Delpuech, Practical NMR Spectroscopy, Heydn and Son (London, 1980).
2. P. C. Lauterbur, "Image Formation by Induced Local Interactions: Examples Employing Nuclear Magnetic Resonance", Nature 242, 190-191 (1973).
3. P. C. Lauterbur, "Medical Imaging by Nuclear Magnetic Resonance Zeugmatography", IEEE Trans. Nucl. Sci. NS-26 (2), 2808-2811 (1979).
4. W. S. Moore, G. N. Holland and L. Kreel, "The NMR CAT Scanner - A New Look at the Brain", CT:the Journal of Computed Tomography, 4 (1), 1-7 (1980).
5. T. C. Farrar and E. D. Becker, Pulse and Fourier Transform NMR, Academic Press (New York, 1971).
6. J. Radon (1917), "Uber die Bestimmung von Functionen durch ihre Intergralwerte langs gewisser Manigfaltigkeiten", Ber. Verh. Sach. Akad. Wiss. Leipzig, 69, 262-277.
7. A. M. Cormack, "Reconstruction of Densities from their Projections, with Applications in Radiological Physics", Phys. Med. Biol. 18 (2), 195 (1973).
8. C.-N. Chen, C.-M. Lai, and P. C. Lauterbur, "NMR Zeugmatography by Three-Dimensional Reconstruction", presented at the VI International Symposium on Magnetic Resonance, Banff, Alberta, Canada, 1977, to be published.
9. P. C. Lauterbur and C.-M. Lai, "Zeugmatography by Reconstruction from Projections" IEEE Trans. Nucl. Sci. NS-27 (3) 1227-1231 (1980).
10. C.-N. Chen, "Direct Three-Dimensional Image Reconstructions from Plane Integrals and Their Applications in Nuclear Magnetic Resonance Zeugmatography" Part I of Ph.D. dissertation, Chemistry Department, SUNY Stony Brook (August 1980).
11. C.-N. Chen, R. B. Marr, and P. C. Lauterbur, "Direct Methods for Three Dimensional Reconstruction in NMR Zeugmatography", to be published.
12. L. A. Shepp, "Computerized Tomography and Nuclear Magnetic Resonance", J. Comput. Assist. Tomogr. 4 (1), 94-107 (1980).

13. D. Ludwig (1966), "The Radon Transform on Euclidean Spaces", Comm. Pure. Appl. Math., 19, 49-81.
14. M. Davison and F. A. Grunbaum (1979), "Convolution Algorithms for Arbitrary Projection Angles", IEEE Trans. Nucl. Sci., NS26, 2670-2673.
15. F. A. Grunbaum, "Reconstruction with Arbitrary Directions: Dimensions Two and Three", (These Proceedings).
16. G. N. Ramachandran and A. V. Lakshminarayanan (1971), "Three-Dimensional Reconstruction from Radiographs and Electron Micrographs: Application of Convolutions instead of Fourier Transforms", Proc. Natl. Acad. Sci. U.S., 68 (9), 2236-2240.
17. L. A. Shepp and B. F. Logan (1974), "The Fourier Reconstruction of a Head Section", IEEE Trans. Nucl. Sci., NS-21, 21-43.
18. C.-M. Lai and P. C. Lauterbur, "Microprocessor-Controlled Reorientation of Magnetic Field Gradients for NMR Zeugmatographic Imaging", Chem. Biomed. Environ. Instr. 9, 1-27 (1979).